23. R. W. Carlson and G. W. Lugmair, *ibid.* **52**, 227 (1981).
24. O. Eugster, J. Geiss, N. Grögler, *Lunar Planet. Sci.* **XIV**, 177 (1983).
25. I. Kaneoka and N. Takaoka, *Mem. Natl. Inst. Polar Res. Spec. Issue* **41**, 116 (1986).
26. N. Takaoka, *ibid.*, p. 124.
27. D. D. Bogard and P. Johnson, *Geophys. Res. Lett.* **10**, 801 (1983).
28. O. Eugster, J. Geiss, U. Krähenbühl, S. Niedermann, *Earth Planet. Sci. Lett.* **78**, 139 (1986).
29. R. Ostertag *et al.*, *Mem. Natl. Inst. Polar Res. Spec. Issue* **41**, 17 (1986).
30. G. W. Wetherill, in *Origin and Distribution of the Elements*, L. H. Ahrens, Ed. (Pergamon, New York, 1968), pp. 423–443.
31. P. Englert and W. Herr, *Earth Planet. Sci. Lett.* **47**, 361 (1980).
32. R. C. Reedy, J. R. Arnold, D. Lal, *Science* **219**, 127 (1983).
33. C. Tuniz *et al.*, *Geophys. Res. Lett.* **10**, 804 (1983).
34. K. Nishiizumi, R. C. Reedy, J. R. Arnold, *Meteoritics* **23**, 294 (1988).
35. N. Takaoka, *Mem. Natl. Inst. Polar Res. Spec. Issue* **46**, 96 (1987).
36. S. R. Sutton and G. Crozaz, *Geophys. Res. Lett.* **10**, 809 (1983).
37. S. R. Sutton, *Mem. Natl. Inst. Polar Res. Spec. Issue* **41**, 133 (1986).
38. K. Nishiizumi *et al.*, in *Papers presented at the 11th NIPR Symposium on Antarctic Meteorites*, K. Yanai, Ed. (NIPR, Tokyo, 1986), pp. 58–59.
39. W. A. Cassidy and L. A. Rancitelli, *Am. Sci.* **70** (no. 2), 156 (1982).
40. T. Fukuoka, J. C. Laul, M. R. Smith, R. A. Schmitt, in *Papers Presented at the 11th NIPR Symposium on Antarctic Meteorites*, K. Yanai, Ed. (NIPR, Tokyo, 1986), pp. 40–42.
41. K. Yanai, H. Kojima, S. Ikadi, *ibid.*, pp. 25–27.
42. K. Yanai and H. Kojima, in *Papers Presented at the 12th NIPR Symposium on Antarctic Meteorites*, K. Yanai, Ed. (NIPR, Tokyo, 1987), p. 3.
43. For the production of the stable noble gas isotopes, an exposure during 10.7 million years in free space (4π exposure to cosmic rays) in equivalent to an exposure during 11.4 million years in the first stage (lunar regolith, 2π exposure) and during 5 million years in the late stage (free space). In this model, I assume that exposure to cosmic rays occurred in both stages at the same shielding depth. This appears to be the case as indicated by the depth-sensitive cosmogenic $^{131}Xe/^{126}Xe$ ratio. The ^{131}Xe production increases with depth relative to that of ^{126}Xe because of the reaction of ^{130}Ba with secondary cosmic ray–produced neutrons. In Y-82192 and Y-82193, $^{131}Xe/^{126}Xe$ ratios of 3.4 and 2.7, respectively, were measured (*26*), and Y-86032 yielded a value of 2.6. These ratios correspond to a shielding depth of 15 cm or less in the meteorite or below the lunar surface.
44. P. H. Warren and G. W. Kallemeyn, *Mem. Nat. Inst. Polar Res. Spec. Issue* **41**, 3 (1986).
45. M. M. Lindstrom, R. L. Korotev, R. L. Lindstrom, R. Score, in *Papers presented at the 12th NIPR Symposium on Antarctic Meteorites*, K. Yanai, Ed. (NIPR, Tokyo, 1987), pp. 19–21.
46. H. J. Melosh, *Geology* **13**, 144 (1985).
47. W. K. Hartmann, *Moons and Planets* (Wadsworth, Belmont, CA, ed. 2, 1983), pp. 161–163.
48. P. W. Kaczaral, J. E. Dennison, M. E. Lipschutz, *Mem. Natl. Inst. Polar Res. Spec. Issue* **41**, 76 (1986). C. M. Pieters, B. R. Hawke, M. Gaffey, L. A. McFadden, *Geophys. Res. Lett.* **10**, 813 (1983).
49. K. Takahashi and A. Masuda, *Mem. Natl. Inst. Polar Res. Spec. Issue* **46**, 71 (1987).
50. N. Nakamura, D. M. Unruh, M. Tatsumoto, in *Papers presented at the 10th NIPR Symposium on Antarctic Meteorites*, K. Yanai, Ed. (NIPR, Tokyo, 1985), pp. 103–105.
51. N. Nakamura, D. M. Unruh, M. Tatsumoto, T. Fujiwara, *Lunar Planet. Sci.* **XVII**, 601 (1986).
52. J. H. Chen and G. J. Wasserburg, *ibid.* **XVI**, 119 (1985).
53. I. Kaneoka and N. Takaoka, *Mem. Natl. Inst. Polar Res. Spec. Issue* **46**, 105 (1987).
54. B. Mason, *U.S. Geol. Surv. Prof. Pap.* **440B-1** (1979).
55. K. Nishiizumi *et al.*, *Earth Planet. Sci. Lett.* **62**, 407 (1983).
56. I thank the National Institute of Polar Research in Tokyo for the meteorite sample, B. Aebersold, P. Guggisberg, S. Niedermann, A. Schaller, I. Spellman, T. Velasquez, and M. Zuber for their help at various stages of this work, and J. Geiss and P. Eberhardt for their encouragement. I thank R. C. Reedy for production rate calculations and K. Marti and J. Arnold for many illuminating discussions. This work was supported by the Swiss National Science Foundation.

Experiments with High-Energy Neutrino Beams

J. STEINBERGER

Experiments in which high-energy neutrinos were used as projectiles have made substantial contributions to our understanding of both weak and strong interactions, as well as the structure of hadrons. This article offers some illustrations. It recalls the discovery of the neutral weak current and some experiments on its nature. The sections on charged-current inclusive scattering recall the important role of these experiments in the understanding of the quark structure of the nucleon and the validity of quantum chromodynamics. The section on dimuon production illustrates the role of neutrino experiments in establishing the Glashow-Iliopoulos-Maiani current as well as the measurement of the structure function of the strange quark in the nucleon.

HIGH-ENERGY NEUTRINO BEAMS HAVE FOUND INTENSIVE and varied application in particle physics experimentation in the last decades. In this review I discuss a few of the most fruitful examples: the discovery of neutral currents, the measurement of the Weinberg angle, the study of weak currents and the consequent test of the electroweak theory, the study of nucleon quark structure, and the testing of quantum chromodynamics (QCD). Other studies, such as the production of "prompt" neutrinos, the search for finite neutrino masses and neutrino oscillations, the search for heavy leptons or other new particles, the measurement of proton and neutron structure functions, elastic and pseudoelastic cross sections, and other exclusive processes, are not discussed here. Neutrino experiments have been pursued vigorously at the Brookhaven National Laboratory (BNL), at Fermilab, and at CERN. It is fair to say that they have made large contributions to our understanding of particle physics.

The author is at CERN (European Laboratory for Particle Physics), Geneva, Switzerland, and Scuola Normale Superiore, Pisa, Italy. This article is adapted from the lecture he delivered in Stockholm on 8 December 1988, when he received the Nobel Prize in Physics, which he shared with Mel Schwartz and Leon Lederman. The article is published here with permission from the Nobel Foundation. The article by Dr. Schwartz was published in the issue of 17 March 1989. The article by Dr. Lederman was published in the 12 May 1989 issue.

Neutrino Beams

Present neutrino beams are produced in four steps: (i) production of secondary hadrons in the collision of high-energy protons on a fixed target; (ii) momentum (charge) selection and focusing of the hadrons; (iii) passage of the beam through an (evacuated) decay region, long enough to permit a substantial fraction of the hadrons to decay; and (iv) absorption of the remaining hadrons and the muons that are produced along with the neutrinos in a shield of adequate thickness. The two-body decays $\pi^{+(-)} \rightarrow \mu^{+(-)} + \nu(\bar{\nu})$ and $K^{+(-)} \rightarrow \mu^{+(-)} + \nu(\bar{\nu})$ account for ~97% of the neutrino flux in present beams. Positive hadrons produce neutrinos (ν), negative hadrons produce antineutrinos ($\bar{\nu}$). Figure 1 gives an impression of the two hadron beam–forming options that are available, side by side, at CERN: a conventional, so-called narrow-band beam (NBB), and an achromatic, Van der Meer horn-focused, wide-band beam (WBB). The neutrino spectra produced by these two beams are very different. The WBBs are characterized by high intensity, a steep (generally undesirable) energy falloff, and a substantial contamination of wrong-"sign" neutrinos. The NBBs have lower intensity, a flat energy dependence in the contribution from each of the two decays, and small wrong-sign background. They also have the important feature that the energy of the neutrino can be known, subject to a twofold π-K dichotomy, if the decay angle is known. In general, this can be inferred from the impact parameter of the event in the detector.

Detectors

The low cross sections of neutrinos are reflected in two general features of neutrino detectors: (i) they are massive and (ii) the target serves also as a detector. In the 1970s, the most successful detectors were large bubble chambers. The most splendid of these were the cryogenic devices built at CERN and Fermilab, each with a volume of ~15 m^3, in large magnetic fields, and capable of operating with liquid hydrogen, deuterium, or neon. A typical neutrino event in the CERN chamber is shown in Fig. 2. It is an example of the "charged current" (CC) reaction $\nu + N \rightarrow \mu^- +$ hadrons. However, one of the major discoveries at CERN was made not in this chamber but in a large Freon-filled bubble chamber, affectionately called Gargamelle. The active volume was a cylinder 4.8 m long and 1.9 m in diameter, for a volume of about 13 m^3, inside a magnet producing a field of 2 T.

The bubble chamber has now been largely replaced by detectors

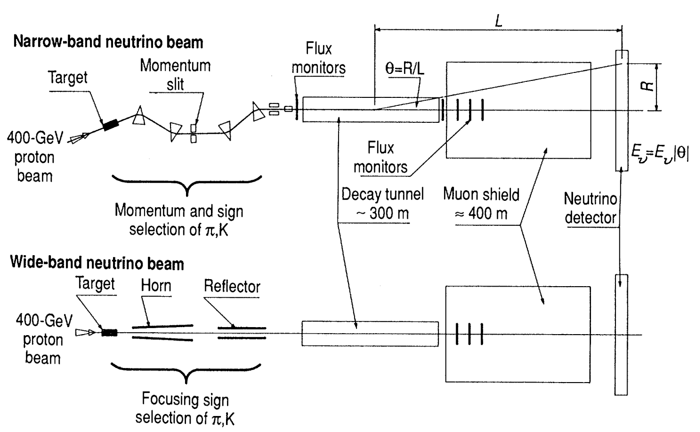

Fig. 1. Sketch of the narrow-band and wide-band neutrino beam layouts at CERN, showing the disposition of the primary target, the focusing elements, the decay region, the shielding, and the monitoring devices.

Fig. 2. A typical neutrino event as observed at the Big European Bubble Chamber filled with neon at the CERN 450-GeV super proton synchrotron accelerator. The muon may be seen at the left; it has been tagged by an external muon identifier. The many-particle hadron shower is to the right.

based on electronic detection methods. As an example, I mention here the CDHS (CERN-Dortmund-Heidelberg-Saclay Collaboration) detector used at CERN from 1977 to 1985. It consists of 19 modules made of iron plates 3.75 m in diameter, each with total iron thickness of 75 cm and a weight of ~65 tons. The iron is toroidally magnetized to a field of 1.7 T by means of coils that pass through a hole in the center.

Interleaved with the 5-cm-thick iron plates are scintillator strips, which serve to measure the energy of the secondary hadrons by sampling the ionization. The typical hadron shower is ~25 cm in radius and ~1 m long, so the shower dimensions are very small compared with the size of the detector. The muon momenta are determined on the basis of curvature in the magnetic field, with the help of drift chambers inserted between the iron modules. These measure the positions of traversing tracks in three projections. The useful target weight is ~800 tons.

Neutral Currents

Discovery. The evolution of the electroweak unified gauge theory in the late 1960s and early 1970s was a remarkable achievement but one that had no immediate impact on the majority of particle physicists—certainly not on me—perhaps because it was a theoretical construct, which left the existing experimental domain intact. However, it predicted some entirely new phenomena, and of these the neutral weak currents were the first to be discovered. The verification of neutral currents (NCs) established the theory overnight, and subsequent experiments on their detailed structure reinforced it. This observation (*1*) of neutral weak currents in 1973 by the Gargamelle group was the first great discovery made at CERN. It was followed 10 years later by the second—also a prediction of the same theory—the intermediate boson.

The bubble chamber, built under the direction of A. Lagarrigue at the École Polytechnique in Paris, was exposed to neutrino and antineutrino WBBs at the CERN 24-GeV proton accelerator. The normal CC reactions,

$$\nu(\bar{\nu}) + N \rightarrow \mu^-(\mu^+) + \text{hadrons}$$

were found as usual, but NC "muonless" reactions,

$$\nu(\bar{\nu}) + N \rightarrow \nu(\nu) + \text{hadrons}$$

which had hardly been looked for before, and therefore had not been found, were there as well. Such an event is shown in Fig. 3A. These events were selected on the basis of no muon candidate among the observed particles. The main experimental challenge was to show that they were not due to stray neutrons in the beam. I myself was a skeptic for a long time, and I lost a number of wagers (a bottle or two of good wine) over this matter. However, the neutron background would be expected to decrease exponentially along the length of the chamber, roughly with the neutron mean free path in Freon. Instead, the event distribution was flat, as expected for neutrino events (see Fig. 3B). I have never enjoyed paying a debt more than at the dinner we gave for the winners, Jacques Prentki, John Iliopoulos, and Henri Epstein.

The ratios of the cross sections

$$R_\nu = \frac{\sigma_\nu^{NC}}{\sigma_\nu^{CC}}$$

and

$$R_\nu = \frac{\sigma_{\bar\nu}^{NC}}{\sigma_{\bar\nu}^{CC}}$$

are given in the electroweak theory in terms of the Weinberg angle, θ_w:

$$R_\nu = \frac{1}{2} - \sin^2\theta_w + (1 + r)\,\frac{5}{9}\,\sin^4\theta_w \tag{1}$$

and

$$R_{\bar\nu} = \frac{1}{2} - \sin^2\theta_w + \left(1 + \frac{1}{r}\right)\frac{5}{9}\,\sin^4\theta_w \tag{2}$$

where r is the ratio of antineutrino to neutrino CC total cross sections: $r = \sigma^{CC,\bar\nu}/\sigma^{CC,\nu} = 0.48 \pm 0.02$ experimentally. On the basis of these ratios, the experiment yielded a first measure of $\sin^2\theta_w$ that was not very different from present, more precise determinations. In the same exposure an excellent example of another NC process, the scattering of an antineutrino on an electron, was also found (*2*).

Precision measurement of $\sin^2\theta_w$ and right-handed neutral currents. The higher energies that became available a few years later at Fermilab and CERN made the study of NC processes much easier. The muons of the CC background now had a greater penetration power, which permitted cleaner separation of NC and CC events. Also, with the advent of the higher energies, the advantage in the study of inclusive neutrino scattering had shifted to electronic detection techniques. In the period 1977 to 1985, hadronic NC neutrino scattering was studied extensively by the CDHS Collaboration at CERN in order to obtain a more precise value for θ_w (*3*) and to check the prediction of the electroweak theory for the ratio of right-handed to left-handed NCs (*4*). The NC events are selected on the basis of short event length, that is, the short penetration of the hadronic shower compared with that of the muon of CC events. A 15% background of CC events is subtracted. The neutrino NC to CC ratio R_ν yielded the most precise value of the weak mixing angle available at present, $\sin^2\theta_w = 0.227 \pm 0.006$. Once $\sin^2\theta_w$ is known, the antineutrino ratio $R_{\bar\nu}$ follows from Eq. 2. Its measurement provided a sensitive test of the electroweak theory and

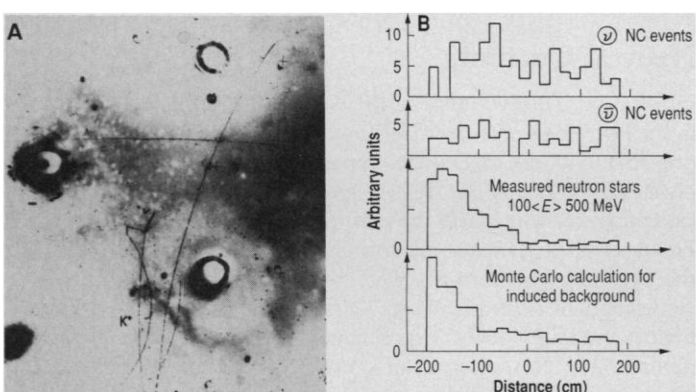

Fig. 3. (**A**) A "muonless" event in Gargamelle. All tracks stop or interact in the chamber. None could be a muon. The neutrino produces one K^+ and one K^0 meson. The K^+ meson interacts in the liquid and then decays. The invisible K^0 meson decays to two pions. (**B**) Distribution of the origin of muonless events along the beam direction in Gargamelle. Neutrino events are expected to be uniformly distributed, whereas neutron events should decrease with distance because of their absorption in the Freon. The nuclear mean free path in Freon is about 80 cm. The expected and observed distributions of neutron interactions are shown in the bottom two histograms. The muonless events are consistent with neutrino and inconsistent with neutron origin (*1*).

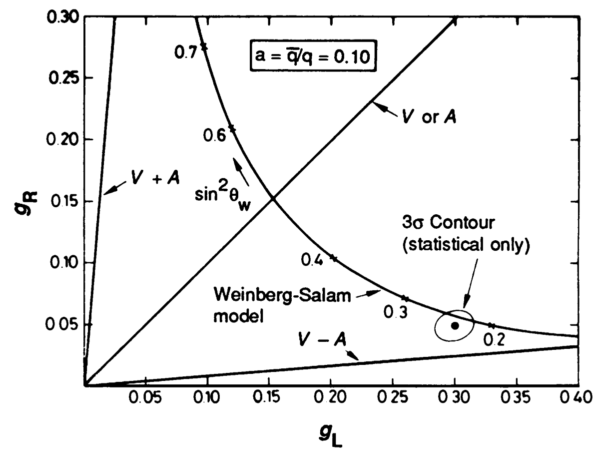

Fig. 4. Strengths of the left- and right-handed NCs; g_L and g_R are the left- and right-handed coupling strengths, respectively. If the NC were purely left-handed, as is the case for the CC, the experimental point would be expected to fall on the $V - A$ line. The experiment shows a right-handed component, which is just that expected in the electroweak theory (Weinberg-Salam model) (*4*).

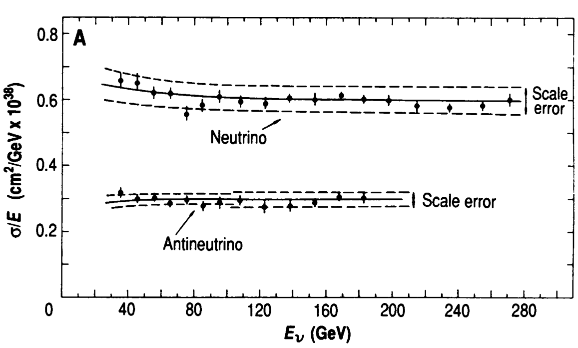

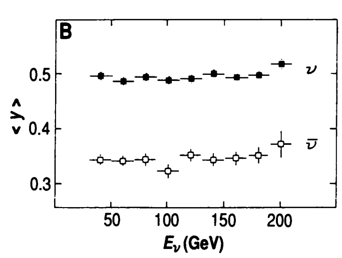

Fig. 5. (**A**) Total neutrino and antineutrino cross sections per nucleon divided by neutrino energy. The flat "scaling" behavior is a consequence of the point-like interaction of the constituents (*10*). (**B**) The average of y (the fraction of the neutrino energy transmitted to the final hadron state) as a function of the neutrino energy, for neutrinos and antineutrinos. The uniformity is a consequence of scaling, which in turn is a consequence of the point-like interaction of the quark (*10*).

confirmed it in its simplest form. The presence of right-handed NCs (CCs are purely left-handed) in the amount predicted by the theory could be demonstrated by comparing the hadron energy distributions of the NC and CC processes. The result is shown in Fig. 4.

Neutrino-electron scattering. The elastic-scattering reactions of neutrinos on atomic electrons

$$\nu_\mu + e^- \rightarrow \nu_\mu + e^-$$

and

$$\bar{\nu}_\mu + e^- \rightarrow \bar{\nu}_\mu - e^-$$

proceed via NCs. They are characterized by small cross sections—smaller than their hadronic counterparts by the mass ratio m_e/m_p because of the smaller center-of-mass energies—and, for the same reason, by small electron production angles, $\theta_e \approx \sqrt{m_e/E_\nu}$. Until now, these angles have not been resolved by the experiments, so only total cross sections have been measured. The expectations in the electroweak theory are:

$$\sigma^{\nu,e} = \frac{G_F^2 E m_e}{\pi}\left(1 - 4\sin^2\theta_w - \frac{16}{3}\sin^4\theta_w\right)$$

and

$$\sigma^{\bar{\nu},e} = \frac{G_F^2 E m_e}{\pi}\left(\frac{1}{3} - \frac{4}{3}\sin^2\theta_w - \frac{16}{3}\sin^4\theta_w\right)$$

These reactions can also serve to test this theory and have the advantage that strongly interacting particles are not involved, so that the understanding of strong-interaction corrections is not necessary in the interpretation. They have the experimental disadvantage of low rates and consequent large background. The best results at present are from a BNL experiment (*5*) in which relatively low-energy neutrinos, $E \approx 1.5$ GeV, and a 140-ton detector entirely composed of many layers of plastic scintillator and drift chambers were used. The background is subtracted on the basis of the distribution in the production angle of the electron shower. Instead of comparing the neutrino and antineutrino cross sections directly with the theory, the investigators form the ratio of the two, which is less sensitive to some systematic errors. From this they find that $\sin^2\theta_w = 0.209 \pm 0.032$. A CERN group reports a similar result (*6*), with $\sin^2\theta_w = 0.211 \pm 0.037$. The agreement with other methods of obtaining this angle is an important confirmation of the theory. A massive experiment to improve the precision is currently under way at CERN.

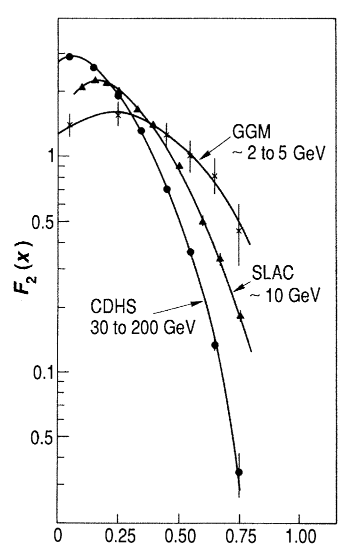

Fig. 6. Scaling is only approximately true for the structure functions. Early measurements of $F_2(x)$ in three different energy domains, CDHS, SLAC, and Gargamelle (GGM), exhibit shrinking, as expected in the QCD theory.

Neutrino-Nucleon Inclusive Scattering and the Quark Structure of Hadrons

Phenomenology. We consider the CC reactions,

$$\nu + N \rightarrow \mu^- + \text{hadrons}$$

and

$$\bar{\nu} + N \rightarrow \mu^+ + \text{hadrons}$$

independently of the final hadron configuration. This is called the inclusive process. It is assumed that the lepton vertex is described by the vector − axial vector current of the electroweak theory. Let k be the initial and k' be the final lepton energy-momentum four vectors, p that of the incident nucleon, and p' that of the final hadron state:

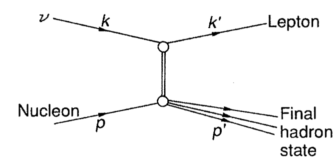

Define the kinematic variables:

$$\begin{aligned}
q &\equiv k - k' \\
Q^2 &\equiv -(k - k')^2 = 4EE'\sin^2\theta/2 \\
\nu &\equiv p \cdot q/m_p = E_h - m_p \simeq E_h \\
x &\equiv q^2/2m_p\nu,\ 0 \leq x \leq 1 \\
y &\equiv \nu/E \simeq E_h/E,\ 0 \leq y \leq 1
\end{aligned}$$

where E and E' are the energies of the initial neutrino and final muon, respectively, θ is the angle between these, and E_h is the energy of the final-state hadrons, all in the laboratory system. The cross sections can be written in terms of three structure functions, each a function of the variables x and Q^2 that characterize the hadronic vertex:

$$\frac{d^2\sigma^{\nu(\bar{\nu})}}{dxdy} = \frac{G^2 m_p E_\nu}{2\pi}\{F_2(x,Q^2)[1 + (1-y)^2] - y^2F_L(x,Q^2) \overset{+}{\underset{(-)}{}} xF_3(x,Q^2)[1 - (1-y)^2]\}$$

The sum of neutrino and antineutrino cross sections has the same structure-function dependence as does the cross section for charged leptons:

$$\frac{d^2\sigma^{\ell\pm}}{dxdy} = \frac{2\pi\alpha^2 m_p E}{Q^4}\{F_2{}^{\ell\pm}(x,Q^2)[1 + (1-y)^2] - y^2F_L(x,Q^2)\}$$

Quark structure of the nucleon. In 1969, at the newly completed 2-mile linear electron accelerator at Stanford (SLAC), it was discovered (*7*) that in electron-proton collisions, at high momentum transfer, the form factors were independent of Q^2. This so-called "scaling" behavior is characteristic of "point," or structureless, particles. The interpretation in terms of a composite structure of the protons, that is, protons composed of point-like quarks, was given by Bjorken (*8*) and Feynmann (*9*).

Neutrinos are projectiles par excellence for investigating this structure, in part because of the heavy mass of the intermediate boson and in part because quarks and antiquarks are scattered differently by neutrinos owing to the vector–axial vector character of the weak currents; they can therefore be distinguished in neutrino scattering, whereas in charged-lepton scattering this is not possible. The quark model makes definite predictions for neutrino-hadron scattering, which are confirmed experimentally. Many of the predic-

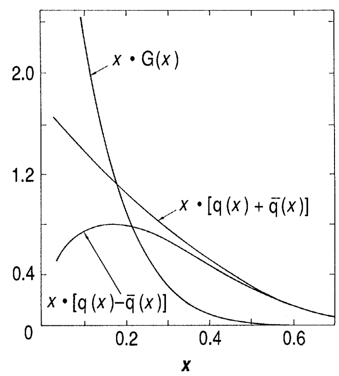

Fig. 7. The gluon distribution $G(x)$ derived from the QCD fits to $F_2(x, Q^2)$, $\bar{q}(x, Q^2)$, and $xF_3(x, Q^2)$ (*10*).

tions rest on the fact that now the kinematic variable x takes on a physical meaning: it can be interpreted as the fraction of the nucleon momentum or mass carried by the quark on which the scattering takes place. In the neutrino experiments I review here iron primarily has been used as the target material. Iron has roughly equal numbers of protons and neutrons. For such nuclei, the cross sections can be expressed in terms of the total quark and total antiquark distributions in the proton. Let $u(x)$, $d(x)$, $s(x)$, $c(x)$, . . . , be the up, down, strange, charm, . . . , quark distributions in the proton. The proton contains three "valence" quarks: two up-quarks and one down-quark. In addition, it contains a "sea" of virtual quark-antiquark pairs. The up valence-quark distribution is $u(x) - \bar{u}(x)$, and the down valence-quark distribution is $d(x) - \bar{d}(x)$. The sea quarks and antiquarks have necessarily identical distributions, so that $s(x) = \bar{s}(x)$, $c(x) = \bar{c}(x)$, and so forth. For the neutron, u and d change roles, but s and c are the same. Let

$$q(x) = u(x) + d(x) + s(x) + c(x) + \ldots$$

and

$$\bar{q}(x) = \bar{u}(x) + \bar{d}(x) + \bar{s}(x) + \bar{c}(x) + \ldots$$

be the total quark and antiquark distributions of the proton, respectively. For spin-½ quarks interacting according to the standard model, for a target with equal numbers of protons and neutrons, and for $Q^2 \ll m_w^2$ and $m_p \ll E$:

$$\frac{d^2\sigma^{\nu}}{dxdy} = \frac{G_F^2 E m_p}{\pi} x[q(x) + (1 - y)^2 \bar{q}(x)]$$

and

$$\frac{d^2\sigma^{\bar{\nu}}}{dxdy} = \frac{G_F^2 E m_p}{\pi} x[\bar{q}(x) + (1 - y)^2 q(x)]$$

Comparison with the expression for the cross section in terms of structure functions then gives these functions in terms of quark distributions:

$$F_2(x,Q^2) = x[q(x) + \bar{q}(x)]$$

$q(x) + \bar{q}(x)$ is the total quark + antiquark distribution;

$$xF_3(x,Q^2) = x[q(x) - \bar{q}(x)]$$

$q(x) - \bar{q}(x)$ is the "valence"-quark distribution;

$$F_L(x,Q^2) = 0$$

this is a consequence of the spin-½ nature of the quarks. From these simple expressions for the cross sections, in terms of quark structure, several tests of the quark model are derived. For the experimental comparisons, we take the CDHS experiments (*10*). The measurements in the detector, that is, the hadron energy and the muon momentum, are just sufficient to define the inclusive process.

1) Scaling. The independence of the differential cross sections with respect to Q^2 is evident everywhere, over a large domain in Q^2. As one example, Fig. 5A shows the linearity of the total cross sections with neutrino energy; as another, Fig. 5B shows the uniformity of the average of y with respect to neutrino energy; both examples are consequences of scaling. Small deviations from scaling are observed in the structure functions, as we will see later, but these are due to the strong interactions of the quarks.

2) The y dependence of the cross sections. We expect

$$\frac{d\sigma^{\nu}}{dy} + \frac{d\sigma^{\bar{\nu}}}{dy} \propto [1 + (1 - y)^2] \int x[(q(x) + \bar{q}(x)]dx$$

and

$$\frac{d\sigma^{\nu}}{dy} - \frac{d\sigma^{\bar{\nu}}}{dy} \propto [1 - (1 - y)^2] \int x[q(x) - \bar{q}(x)]dx$$

The agreement with this expectation is quite good. A corollary of this agreement is that $F_L(x)$ is small. It is found that $\int F_L(x)dx / \int F_2(x)dx \simeq 0.1$. Here also, this deviation from the simple quark picture is understood in terms of the strong interactions of the quarks, as we will see later.

3) Correspondent between $F_2^{\ell\pm}(y)$ and $F_2^{\nu}(x)$. Both are proportional to $q(x) + \bar{q}(x)$ and so are expected to have the same x dependence in the simple quark model. They are related by the factor

$$\frac{F_2^{\ell\pm}(x)}{F_2^{\nu}(x)} = \frac{1}{2}\left[\left(\frac{2}{3}\right)^2 + \left(-\frac{1}{3}\right)^2\right] = \frac{5}{18}$$

Here ⅔ and −⅓ are the up- and down-quark electric charges, respectively. The agreement in shape and magnitude not only supports the quark picture but also demonstrates the third integral quark electric charge.

4) $\int xF_3(x)\,dx/x = 3$. Because $xF_3(x) = x[q(x) - \bar{q}(x)]$ in the quark model and $q(x) - \bar{q}(x)$ is the valence-quark distribution, this sum rule states that there are three valence quarks in the nucleon. The experimental demonstration is not without problems, because the ν and $\bar{\nu}$ cross sections are finite as x goes to 0, and the difference, which is $xF_3(x)$, has a consequent large error at small x, which is divided by x as x goes to 0. However, all experiments give a value near 3, with typical uncertainties of ~10%.

Taken together with the charged-lepton inclusive scattering experiments, the neutrino experiments leave no doubt about the validity of the quark picture of nucleon structure. In addition, the neutrino experiments are unique in offering the possibility of measuring independently the quark and antiquark distributions in the nucleon.

If the quarks were the sole nucleon constituents, we would expect $\int F_2(x)dx = \int x[q(x) + \bar{q}(x)]dx$ to be equal to 1. Experimentally, $\int F_2(x)dx = 0.48 \pm 0.02$. We should have expected that some of the nucleon momentum is carried by the gluons, the mesons that bind the quarks. The experimental result is therefore interpreted to mean that gluons account for about half of the nucleon momentum (or mass).

Neutrino scattering and QCD. QCD is the elegant new gauge theory of the interaction of quarks and gluons, which describes the binding of quarks into the hadrons. Deep-inelastic lepton scattering provided a means of testing the predictions of this important theory and gave it its first experimental support. So far, no one has succeeded in calculating low-energy hadronic phenomena such as the wave functions of quarks in hadrons, because of the large coupling constant that frustrates perturbation methods at low energy. At high Q^2, however, the effective coupling constant becomes logarithmically smaller, and perturbation calculations become credible. The theory predicts "scaling violations" in the form of a "shrinking" of the structure functions toward smaller x as Q^2 becomes larger. This is observed experimentally, as can be seen from Fig. 6. In the theory, the shrinking is the consequence of the emission of gluons in the scattering process. This emission can be calculated. The Q^2 evolution at sufficiently high Q^2 is therefore quantitatively predicted by the theory. In neutrino experiments this Q^2 evolution could be measured, and these measurements confirmed the theory and contributed to its acceptance. In the case of xF_3, the theoretical predictions have only one free parameter, the coupling constant, α_s. In the case of F_2, the Q^2 evolution is coupled to the gluon distribution $G(x,Q^2)$. The theory fits the data adequately. These fits give a value for the parameter Λ in the running strong-coupling constant,

$$\alpha_s = [6/(33 - 2N_f) \ln (Q^2/\Lambda^2)]$$

where N_f is the number of excited quark flavors ($N_f \simeq 4$ in this experiment) and $\Lambda \simeq 100$ MeV. They also give the gluon distribution shown in Fig. 7. These QCD comparisons suffer somewhat from the fact that Q^2 is still too low to reduce nonperturbative effects to a negligible level, but the calculable perturbative effects dominate and are confirmed by the experiments. Perturbative QCD also predicts a nonzero longitudinal structure function $F_L(x,Q^2)$ as another consequence of the emission of gluons. This prediction is compared with the CDHS experimental results in Fig. 8. Here also, the experiment lends support to the theory.

Neutrino Interactions, GIM Weak Current, and the Strange Quark in the Nucleon

Among the most exciting results obtained with neutrino beam experiments are those concerning the opposite-sign "dimuons" first observed at Fermilab (*11*) and studied in detail in the CDHS experiments (*12*). These reactions occur at roughly 1/100 of the rate of the dominant single-muon events. The experiments are interesting, on the one hand because they confirm the doublet structure of the quark weak current proposed some years ago by Glashow, Iliopoulos, and Maiani (GIM) (*13*), and which is fundamental to the electroweak theory, and on the other hand because they give such a vivid confirmation of the nucleon quark structure altogether.

The origin of the extra muon was quickly understood as being due to the production of charmed quarks and their subsequent muonic decay. In the GIM model, the charm-producing reactions are

		GIM cross section proportionality	
$\nu + d \rightarrow \mu^- + c;$	$c \rightarrow \mu^+ + \ldots$	$xd(x) \sin^2 \theta_c$	(3)
$\nu + s \rightarrow \mu^- + c;$	$c \rightarrow \mu^+ + \ldots$	$xs(x) \cos^2 \theta_c$	(4)
and			
$\bar{\nu} + \bar{d} \rightarrow \mu^+ + \bar{c};$	$c \rightarrow \mu^- + \ldots$	$x\bar{d}(x) \sin^2 \theta_c$	(5)
$\bar{\nu} + \bar{s} \rightarrow \mu^+ + \bar{c};$	$\bar{c} \rightarrow \mu^- + \ldots$	$x\bar{s}(x) \cos^2 \theta_c$	(6)

The identification of the extra muon events with charm decay is experimentally confirmed in a number of ways: (i) opposite-sign muons are produced, like-sign ones are not; (ii) in general, the extra muon has little energy; (iii) the extra muon is correlated, as expected, to the direction of the hadron shower, of which the charmed particle is a part.

The GIM paper (*13*) preceded the experimental discovery of charm by 5 years. Charm was proposed because of the theoretical attractiveness of the doublet structure of the weak currents. The predictions were precise. The cross sections are proportional to $\sin^2 \theta_c$ for d and $\bar{d}$ quarks and to $\cos^2 \theta_c$ for s and $\bar{s}$ quarks. The Cabibbo angle θ_c was previously known, with $\cos^2\theta_c = 0.95$, close to 1, and $\sin^2\theta_c = 0.05$, very much smaller. Reactions 3 and 4, or 5 and 6, are not experimentally separable because the target nucleon contains both s and d quarks, and the final state is the same. In the antineutrino case, reaction 6 dominates reaction 5 because $\sin^2\theta_c$ is so small. For each event, x and y are measured as for single-muon events. Therefore, the x distribution for antineutrino dimuon production, shown in Fig. 9A, measures the amount and the shape of the strange sea $s(x)$.

In the neutrino reactions, the smallness of $\sin^2\theta_c$ for reaction 3 is very closely compensated by the fact that $d(x)$, containing also

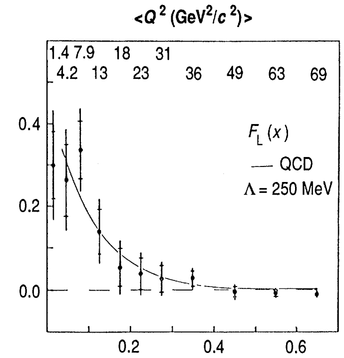

Fig. 8. The structure function $F_L(x)$ associated with longitudinally polarized intermediate bosons, and the QCD predictions. In the simple quark model, F_L is zero (*10*).

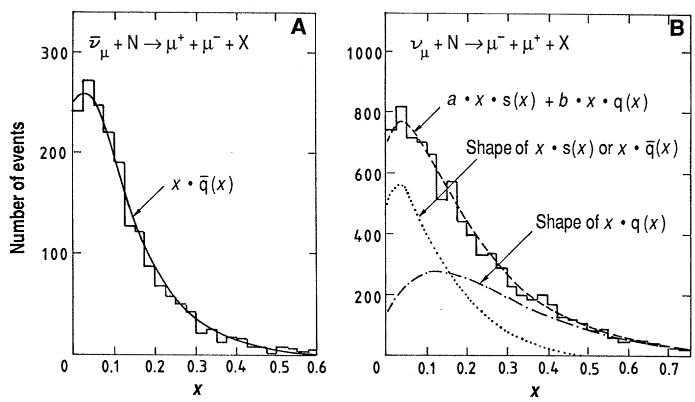

Fig. 9. The x distributions of opposite-sign dimuon events. (**A**) For antineutrinos. The dominant process is $\bar{\nu} + \bar{s} \rightarrow \mu^+ + \bar{c}$. The observed x distribution is therefore that of the strange sea in the nucleon. (**B**) For neutrinos. The process is $\nu + s \rightarrow \mu^- + c$. The shape allows the determination of the relative contributions of s and d quarks and therefore the relative coupling constant. This confirmed the GIM prediction (*12*).

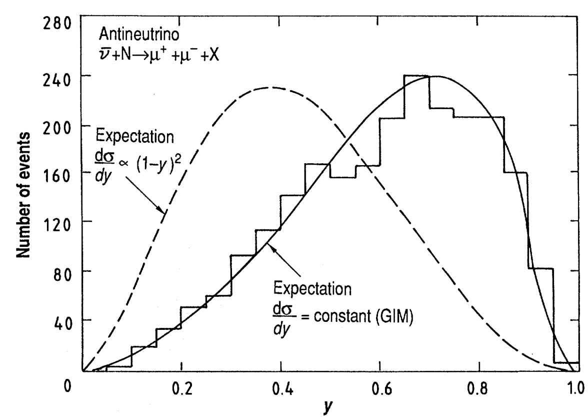

Fig. 10. The y distribution of $\bar{\nu}$-produced dimuons. The acceptance over the y domain is unfortunately very nonuniform, because of the 5-GeV minimum energy required of each muon. The observed y distribution agrees with an acceptance-corrected flat y distribution as predicted by the GIM current but differs strikingly from the $(1 - y)^2$ distribution characteristic of the single-muon antineutrino cross section (*12*).

valence quarks, is much greater than $s(x)$ of reaction 4. By fitting, it can be seen that the x distribution in Fig. 9B is a roughly equal mixture of $s(x)$ as obtained with the antineutrinos and $d(x)$, previously known from the normal CC reactions. The ratio of the two contributions is a measure of θ_c as it enters the charm production reaction. The Cabibbo angle obtained in this way is found to be equal, within errors, to θ_c measured in strange decays, as proposed in the GIM hypothesis. Further support of the GIM current is provided by the y distributions. They reflect the relative helicities of the neutrino and the struck quark: if the two helicities are the same, as is the case for all four charm-producing reactions, the expected y distribution is flat; if they are opposite, as is the case for instance for $\nu + \bar{q}$ and $\bar{\nu} + q$, the expected distribution is $(1 - y)^2$. Both neutrino and antineutrino single-muon reactions are mixtures of the two. The contrast is especially strong for antineutrinos, where the experimental single-muon y distribution is dominated by $(1 - y)^2$, whereas the dimuon distribution is flat, as shown in Fig. 10, again confirming the GIM picture.

Concluding Remarks

I have given some examples to illustrate the impact of high-energy neutrino research on the progress in particle physics of the past years, both in the field of the weak interactions and in that of nucleon structure. How will this develop in the future? I do not know, of course. The increase of proton accelerator energies into the 10-TeV range will certainly permit better QCD tests than those cited above. In general, however, it can be expected that progress in particle physics will depend more and more on colliders, because of their higher center-of-mass energies. High-energy e-p machines, such as the Hadron-Electron Ring Accelerator (HERA), will permit exploration of inclusive scattering to higher Q^2 domains than will be possible with fixed-target neutrino beams.

However, the fascination with neutrinos and the unanswered questions concerning them, such as their masses, are motivating a broad line of research in astrophysics, accelerator physics, and nuclear physics. One of the first and most important results expected from the two large e^+e^- colliders just coming into operation, the Stanford Linear Collider and the CERN Large Electron-Positron accelerator (LEP), which will produce lots of Z^0 mesons, is the determination of how many families of leptons and quarks there really are. Are there others besides the three already known? This fundamental question will be answered by determining how often the Z^0 decays to neutrinos, even if the masses of the other members of possible additional families are too large to permit their production at these energies.

REFERENCES

1. F. J. Hasert *et al.*, *Phys. Lett. B* **46**, 138 (1973).
2. F. J. Hasert *et al.*, *ibid.*, p. 121.
3. M. Holder *et al.*, *ibid.* **71**, 222 (1977); H. Abramowicz *et al.*, *Z. Phys. C* **28**, 51 (1985); *Phys. Rev. Lett.* **57**, 298 (1986).
4. M. Holder *et al.*, *Phys. Lett. B* **72**, 254 (1977).
5. L. H. Ahrens *et al.*, *Phys. Rev. Lett.* **54**, 18 (1985).
6. J. Dorenbosch *et al.*, in preparation.
7. E. D. Bloom *et al.*, *Phys. Rev. Lett.* **23**, 930 (1969); M. L. Breitenbach *et al.*, *ibid.*, p. 935; E. D. Bloom *et al.*, Stanford preprint SLAC-PUB 796 (1979), paper 7b-17 submitted to the Fifteenth International Conference on High-Energy Physics, Kiev, U.S.S.R., 1970.
8. J. D. Bjorken, *Phys. Rev.* **179**, 1547 (1969).
9. R. P. Feynman, *Photon-Hadron Interactions* (Benjamin, New York, 1972).
10. J. G. H. De Groot *et al.*, *Z. Phys. C* **1**, 143 (1979); H. Abramowicz *et al.*, *ibid.* **12**, 289 (1982); *ibid.* **17**, 283 (1983); in preparation.
11. A. Benvenuti *et al.*, *Phys. Rev. Lett.* **34**, 419 (1975).
12. M. Holder *et al.*, *Phys. Lett. B* **69**, 377 (1977); H. Abramowicz *et al.*, *Z. Phys. C* **15**, 19 (1982).
13. S. L. Glashow, J. Iliopoulos, L. Maiani, *Phys. Rev. D* **2**, 1285 (1970).

"You're supposed to have a ringing in your ears. That's what echo-location is all about."